PLOS ONE

RESEARCH ARTICLE

Depletion of Scleraxis-lineage cells during tendon healing transiently impairs multi-scale restoration of tendon structure during early healing

Antonion Korcari[1,2], **Samantha Muscat**[1], **Elizabeth McGinn**[1,2], **Mark R. Buckley**[1,2], **Alayna E. Loiselle**[1,2]*

1 Department of Orthopaedics & Rehabilitation, Center for Musculoskeletal Research, University of Rochester Medical Center, Rochester, NY, United States of America, **2** Department of Biomedical Engineering, University of Rochester, Rochester, NY, United States of America

* Alayna_Loiselle@URMC.Rochester.edu

Citation: Korcari A, Muscat S, McGinn E, Buckley MR, Loiselle AE (2022) Depletion of Scleraxis-lineage cells during tendon healing transiently impairs multi-scale restoration of tendon structure during early healing. PLoS ONE 17(10): e0274227. https://doi.org/10.1371/journal.pone.0274227

Editor: Kanhaiya Singh, Indiana University Purdue University at Indianapolis, UNITED STATES

Received: April 10, 2022

Accepted: August 23, 2022

Published: October 14, 2022

Data Availability Statement: Sequencing data have been deposited in Gene Expression Omnibus (GEO) under accession code GSE213033. https://www.ncbi.nlm.nih.gov/geo/query/acc.cgi?acc=GSE213033.

Funding: NNIH/ NIAMS R01AR073169 and R01AR077527 to Alayna Loiselle (AEL). The funders had no role in study design, data collection and analysis, decision to publish, or preparation of the manuscript.

Abstract

Tendons are composed of a heterogeneous cell environment, with *Scleraxis*-lineage (Scx^{Lin}) cells being the predominant population. Although Scx^{Lin} cells are required for maintenance of tendon homeostasis, their functions during tendon healing are unknown. To this end, we first characterized the spatiotemporal dynamics of Scx^{Lin} cells during tendon healing, and identified that the overall Scx^{Lin} pool continuously expands up to early remodeling healing phase. To better define the function of Scx^{Lin} cells during the late proliferative phase of healing, we inducibly depleted Scx^{Lin} cells from day 14–18 post-surgery using the Scx-Cre; Rosa-DTR mouse model, with local administration of diphtheria toxin inducing apoptosis of Scx^{Lin} cells in the healing tendon. At D28 post-surgery, Scx^{Lin} cell depleted tendons (DTR^{ScxLin}) had substantial impairments in structure and function, relative to WT, demonstrating the importance of Scx^{Lin} cells during tendon healing. Next, bulk RNAseq was utilized to identify the underlying mechanisms that were impaired with depletion and revealed that Scx^{Lin} depletion induced molecular and morphological stagnation of the healing process at D28. However, this stagnation was transient, such that by D56 tendon mechanics in DTR^{ScxLin} were not significantly different than wildtype repairs. Collectively, these data offer fundamental knowledge on the dynamics and roles of Scx^{Lin} cells during tendon healing.

Introduction

Tendons are dense fibrous tissues that connect muscles to bones to enable skeletal movement and joint stability [1]. Such forces can be transmitted successfully due to tendon's structure, which consists of a highly aligned and organized Collagen I rich matrix. Acute tendon injuries are significant since they account for approximately 30% of all musculoskeletal consultations and despite great advances in surgical and rehabilitation protocols, 30–40% of flexor tendon repairs still result in unsatisfactory outcomes [2–4]. After injury, tendons heal via the

Competing interests: The authors have declared that no competing interests exist.

production of fibrotic scar tissue, characterized by abundant and disorganized extracellular matrix (ECM) [5–12]. Despite efforts to regain pre-injury structure via an on-going remodeling process, the imposed structural and functional deficits are largely permanent. Currently, there are signfiicant knowledge gaps related to the specific cell populations and biological mechanisms responsible for tendon healing [13], and as such, there is a paucity of pharmacological strategies to improve the healing process.

While recent studies have demonstrated heterogeneity of the adult tendon cell environment [7,14,15], nearly all cells in the adult tendon are encompassed by the Scleraxis (*Scx*)-lineage [7], with *Scx*, a basic helix-loop-helix transcription factor, being the most-well characterized tendon marker [16]. Recent work has demonstrated that the overall Scx-lineage pool (Scx^{Lin}, as labelled using the non-inducible Scx-Cre) can be further broken down into different subpopulations during post-natal growth, adult homeostasis, and phases of the tendon healing process as shown using the Scx-Cre^{ERT2} driver [14], while other studies have demonstrated *de novo* activation of *Scx* in response to injury [17]. However, whether these subpopulations make distinct contributions to the healing process are unknown. To begin to address this, we recently demonstrated that depletion of Scx^{Lin} cells from adult tendon prior to injury improved the healing process [7]. Intriguingly, lineage tracing suggested that there was a new population of Scx^{+} cells that was transiently added to the overall Scx^{Lin} pool by D14 post-surgery such that Scx^{Lin} depletion prior to injury had minimal effect on the early phases of healing. In contrast, the impact of Scx^{Lin} depletion prior to injury was more profound during late healing (D28) with a concomitant reduction in the overall Scx^{Lin} pool, and functional improvements in healing. Taken together, although the above studies have shed some light on the potential temporally-distinct roles of the overall Scx^{Lin} pool in tendon healing, there are still significant knowledge gaps in terms of their temporal dynamics and time-dependent functions during tendon healing.

In this study, our first goal was to comprehensively define the dynamics of Scx^{Lin} cells during tendon healing. In specific, we focused on both adult Scx^{Lin} cells (cells that expressed *Scx* during adult tendon homeostasis) as well as cells that express *Scx* in response to the injury using the Scx-GFP reporter. Second, we hypothesized that Scx^{Lin} cells contribute to the bridging of tendon stubs via ECM synthesis, and thus, Scx^{Lin} depletion during the proliferative healing phase will significantly impair the composition, structure, and function of the newly formed bridging tissue.

Materials and methods

Mice

This study was carried out in strict accordance with the recommendations in the Guide for the Care and Use of Laboratory Animals of the National Institutes of Health (Bethesda, MD, USA). All animal procedures were approved by the University Committee on Animal Research (UCAR) at the University of Rochester. *Scx-Cre (*MGI:5317938), *Scx-*Cre^{ERT2} [8,18] and Scx^{GFP} reporter [19,20] mice were generously provided by Dr. Ronen Schweitzer. Scx^{GFP} reporter mice trace and visualize all the cells that are actively expressing *Scx* at the time of harvest. Rosa-Ai9 (#007909) and Rosa-DTR^{LSL} (#007900) mice were obtained from the Jackson Laboratory (Bar Harbor, ME, USA). For the lineage-tracing studies, first, *Scx-*Cre^{ERT2} mice were crossed to Rosa-Ai9 to generate *Scx-*$Cre^{ERT2,Ai9}$ ($Scx^{LinAdult}$)mice. Next, homozygous *Scx-*$Cre^{ERT2,Ai9}$ mice were crossed to $Scx^{GFP/GFP}$ to generate *Scx-*$Cre^{ERT2,Ai9}$;Scx^{GFP} reporter mice. These mice received three 100 mg/kg intraperitoneal (i.p.) tamoxifen (TMX) injections beginning seven days prior to FDL tendon injury and repair surgery to label and trace cells that actively expressed *Scx* during homeostasis (adult Scx^{Lin} cells), while ensuring that no

subsequent labeling occurred during FDL tendon healing by introducing a washout period of four days between the last i.p. TMX injection and the tendon surgeries. In parallel, the GFP reporter in these mice allows for additional labeling and tracing of all cells that actively express *Scx* at the time of harvest. For the depletion studies, *Scx-Cre* mice were crossed to the Rosa-DTR^{LSL} mice to generate *Scx-Cre*$^{+}$*; DTR*$^{F/+}$, a model of broad *Scx*^{Lin} cell depletion (DTR^{ScxLin}) [7,14], while *Scx-Cre*$^{-}$*; DTR*$^{F/+}$ mice were used as wildtype littermates controls (WT). Diphtheria toxin receptor (Rosa-DTR^{LSL}) mice can be utilized to temporally ablate cell populations in a cell/tissue-type specific manner using Cre drivers [21]. The expression of DTR is inhibited prior to Cre-mediated recombination due to the presence of a STOP cassette flanked by loxp site (Loxp-STOP-Loxp; LSL). The STOP cassette is deleted due to the Cre-mediated recombination, which results in the expression of the DTR. In this case, DTR is expressed in the overall *Scx*^{Lin} pool. Administration of diphtheria toxin (DT) to these mice results in targeted cell death of the broad *Scx*^{Lin} pool. Both control (WT) and experimental animals (DTR^{ScxLin}) received DT injections (100ng DT per mouse per day for 5 consecutive days) between D14 and D18 post-surgery and samples were harvested either at D28 or D56 post-surgery. All mouse studies were performed with 10–12 week-old male and female mice. All mouse work (injections, surgeries, harvests) were performed in the morning. Mice were kept in a 12 hr light/dark cycle.

Flexor tendon repair

At 10–12 weeks of age, mice underwent complete transection and repair of the flexor digitorum longus (FDL) tendon in the hind paw as previously described [5]. Briefly, mice received an injection of sustained-release buprenorphine (1mg/kg). Next, they were anesthetized with Ketamine (60 mg/kg) and Xylazine (4 mg/kg). To reduce chances of rupture at the repair site, the FDL tendon was first transected at the myotendinous junction, and the skin was closed with a 5–0 suture. MTJ transection results in a transient decrease in loading, with reintegration of the MTJ observed by D7-10 post-surgery. Following sterilization of the surgery region, a small incision was made on the posterior surface of the hind paw, the FDL tendon was located and completely transected using micro spring-scissors. The tendon was repaired using an 8–0 suture and the skin was closed with a 5–0 suture. Following surgery, animals resumed prior cage activity, food intake, and water consumption.

Paraffin histology and immunofluorescence

Hind paws from *Scx-Cre*^{ERT2,Ai9}*;Scx*^{GFP} reporter mice were harvested prior to tendon surgeries, as well as at D7, 14, 21, 28, 35, and 42 post-surgery. Additionally, hind paws from *Scx-Cre; DTR*$^{F/+}$ were harvested at D28 post-surgery. All hind paws were fixed in 10% neutral buffered formalin (NBF) at room temperature for 72 hr and were subsequently decalcified in Webb Jee EDTA (pH 7.2–7.4) for 14 days at room temperature, processed, and embedded in paraffin. Five-micron sagittal sections were utilized for analysis. For immunofluorescence staining, *Scx-Cre*^{ERT2,Ai9}*;Scx*^{GFP} sections were stained with GFP (1:500, Cat#: MA5-15256, INVITROGEN, Waltham, MA), tdTomato (1:500, Cat#: AB8181, SICGEN, Cantanhede, Portugal), and α-SMA-FITC (1:500, Cat#: F3777, Sigma Life Sciences, St. Louis, MO). *Scx-Cre; DTR*$^{F/+}$ repair sections were stained with Postn (1:300, Cat#: AB215199, ABCAM, Cambridge, United Kingdom). All sections were counterstained with the nuclear DAPI stain and imaged with a VS120 Virtual Slide Microscope (Olympus, Waltham, MA). Additionally, *Scx-Cre; DTR*$^{F/+}$ repair sections were stained with Alcian blue/hematoxylin and Orange G (ABHOG) to assess tissue morphology and collagen deposition. Finally, *Scx-Cre; DTR*$^{F/+}$ repair sections were further imaged using Second Harmonic Generation (SHG) imaging to facilitate collagen organization and deposition.

Quantification of fluorescence

Fluorescent images scanned by the virtual slide scanner were quantified using Visiopharm image analysis software v.6.7.0.2590 (Visiopharm, Hørsholm, Denmark). Automatic segmentation via a threshold classifier was used to define and quantify specific cell populations based on cell number. For the uninjured tendon groups, an ROI at the midsubstance that encapsulates the majority of the tendon tissue was drawn. The total number of cells (DAPI), and the number of cells that express each marker of interest ($Scx^{LinAdult}$+, Scx^{GFP}+) was quantified, and each subpopulation was normalized by total cells per image. For the injured samples, an ROI was drawn to encapsulate both the scar tissue and tendon stubs. The number of fluorescent cells was quantified and normalized to the number of the total cell number (DAPI) to determine percentages of each cell type. For quantification of αSMA^+ staining, the same ROI encapsulating both the scar tissue and tendon stubs was used, and the total image area and the αSMA^+ area were measured. An n = 3–5 was used for all staining quantification, with each sample being an independent biological replicate.

Quantification of biomechanical properties

FDL tendons at D28 post-surgery from DTR^{ScxLin} and WT groups were harvested from the hind paws. Under a dissecting microscope, each tendon was carefully separated at the myotendinous junction (MTJ). The tarsal tunnel was cut, and the tendon was released from the tarsal tunnel, isolated until the bifurcation of the digits and then cut and released. Any additional connective tissues (e.g., muscle) were removed under a dissecting microscope, and the tendon was prepared for uniaxial testing. Sandpaper was placed on each end of the tendon and glued together using cyanoacrylate (Superglue, LOCTITE). The tendon was periodically submerged in PBS to avoid any potential tissue drying. Next, gripped tendons were transferred into a semi-customized uniaxial microtester (eXpert 4000 MicroTester, ADMET, Inc., Norwood MA) [22–25]. The microtester was transferred to an inverted microscope (Olympus BX51, Olympus) to visualize the tendon and quantify the gauge length, width, and thickness. The gauge length of each sample was set as the end-to-end distance between opposing sandpaper edges and was set the same for all samples tested. The cross-section of the tendon was assumed as an ellipse, where the width and thickness of the tissue represents the major axis and the minor axes, respectively. Based on the measured width and thickness of each tendon, the area of the elliptical cross-section was computed. A uniaxial displacement-controlled stretching of 1% strain per second until failure was applied. Load and grip-grip displacement data were recorded and converted to stress-strain data, and the failure mode was tracked for each mechanically tested sample. Stiffness and peak load were calculated based on load-displacement curves, while tangent modulus and peak stress were calculated based on stress-strain curves. Note that this method of computing tangent modulus assumes that stress and strain are uniform within each specimen.

RNA extraction, next generation sequencing (NGS), and data analysis of RNA-seq

FDL tendons (1 tendon per biological sample; N = 3 biological samples per genotype) were harvested at D28 post-surgery and flash frozen in liquid nitrogen. Total RNA was isolated using the Powermasher II (DIAGNOCINE) to homogenize the tissue. RNA was isolated from the extract using Trizol (Life Technologies, Carlsbad, CA) and the RNeasy Plus Micro Kit (Qiagen, Valencia, CA) per manufacturer's recommendations. The total RNA concentration was determined with the NanoDrop 1000 spectrophotometer (NanoDrop, Wilmington, DE)

and RNA quality assessed with the Agilent Bioanalyzer (Agilent, Santa Clara, CA). The RNA integrity number (RIN) for all harvested samples was 7.73 ± 0.22 (mean ± standard deviation). The TruSeq Stranded mRNA Sample Preparation Kit (Illumina, San Diego, CA) was used for next-generation sequencing library construction per manufacturer's protocols. Briefly, mRNA was purified from 200 ng total RNA with oligo-dT magnetic beads and fragmented. First-strand cDNA synthesis was performed with random hexamer priming followed by second-strand cDNA synthesis using dUTP incorporation for strand marking. End repair and 3'adenylation was then performed on the double-stranded cDNA. Illumina adaptors were ligated to both ends of the cDNA and amplified with PCR primers specific to the adaptor sequences to generate cDNA amplicons of approximately 200–500 bp in size. The amplified libraries were hybridized to the Illumina flow cell and single end reads were generated for each sample using Illumina NovaSeq6000. The generated reads were demultiplexed using bcl2fastq version 2.19.0. Data cleaning and quality control was accomplished using FastP version 0.20.0. Read quantification was accomplished using subread-1.6.4 package (featureCounts). Data normalization and differential expression analysis of DTR^{ScxLin} relative to WT at a given time point was performed using DESeq2-1.22.1 with an adjusted p-value threshold of 0.05 on each set of raw expression measures. The 'lfcShrink' method was applied, which moderates log2 fold-changes for lowly expressed genes. DeSeq2 data was uploaded to *Enrichr* (https://maayanlab.cloud/Enrichr/) to perform pathway analysis of the DEGs in DTR^{ScxLin} vs WT. Additionally, StringDB (https://string-db.org/) was utilized to identify potential interactions between the DEGs.

Statistical analysis

Experimental n was based on post-hoc power calculations from our previously published work [7–9]. Regarding the biomechanics of D28 and D56 timepoint, the experimental n reflects the number of samples that were included in the final analysis. A total of 8 out of 27 samples from D28 were excluded (4 due to rupture, 1 due to breakage during prep, and 3 due to slippage during tensile testing). As for D56, a total of 6 out of 18 tendons were excluded (3 due to rupture and 3 due to breakage during prep). GraphPad Prism was utilized to analyze quantitative data and is presented as mean ± standard deviation (Stdev). First, all datasets were assessed for normal distribution using the Shapiro-Wilk normality test. A Mann-Whitney test was utilized when data was not normally distributed (Modulus at D28 and D56). Student's t-test was utilized to compare between normally distributed groups. Two-way ANOVA with Tukey's post-hoc was used to assess differences in cell subpopulations at a given timepoint, while Dunnett's multiple comparison test was used to assess differences in the proportion of a given cell population over time. Mice were randomly selected for specific experimental outcome metrics prior to surgery and quantitative data (ex. fluorescence quantification, biomechanics) were analyzed in a blinded manner. p values ≤ 0.05 were considered significant. * indicates $p<0.05$, ** indicates $p<0.01$, *** indicates $p<0.001$, **** indicates $p<0.0001$.

Results

Scx^{Lin} cells continuously expand during the proliferative phase of healing tendons with additonal cells expressing *Scx*

To understand the dynamics and contributions of Scx^{Lin} cells during both tendon homeostasis and healing, we utilized the inducible *Scx-*$Cre^{ERT2,Ai9}$; Scx^{GFP} reporter (**Fig 1A**) mouse model. Our primary goals here were to understand how $Scx^{LinAdult}$+;Scx^{GFP}+ and Scx^{GFP}+ cells compare to each other at different healing timepoints, how $Scx^{LinAdult}$+;Scx^{GFP}+ cells change during

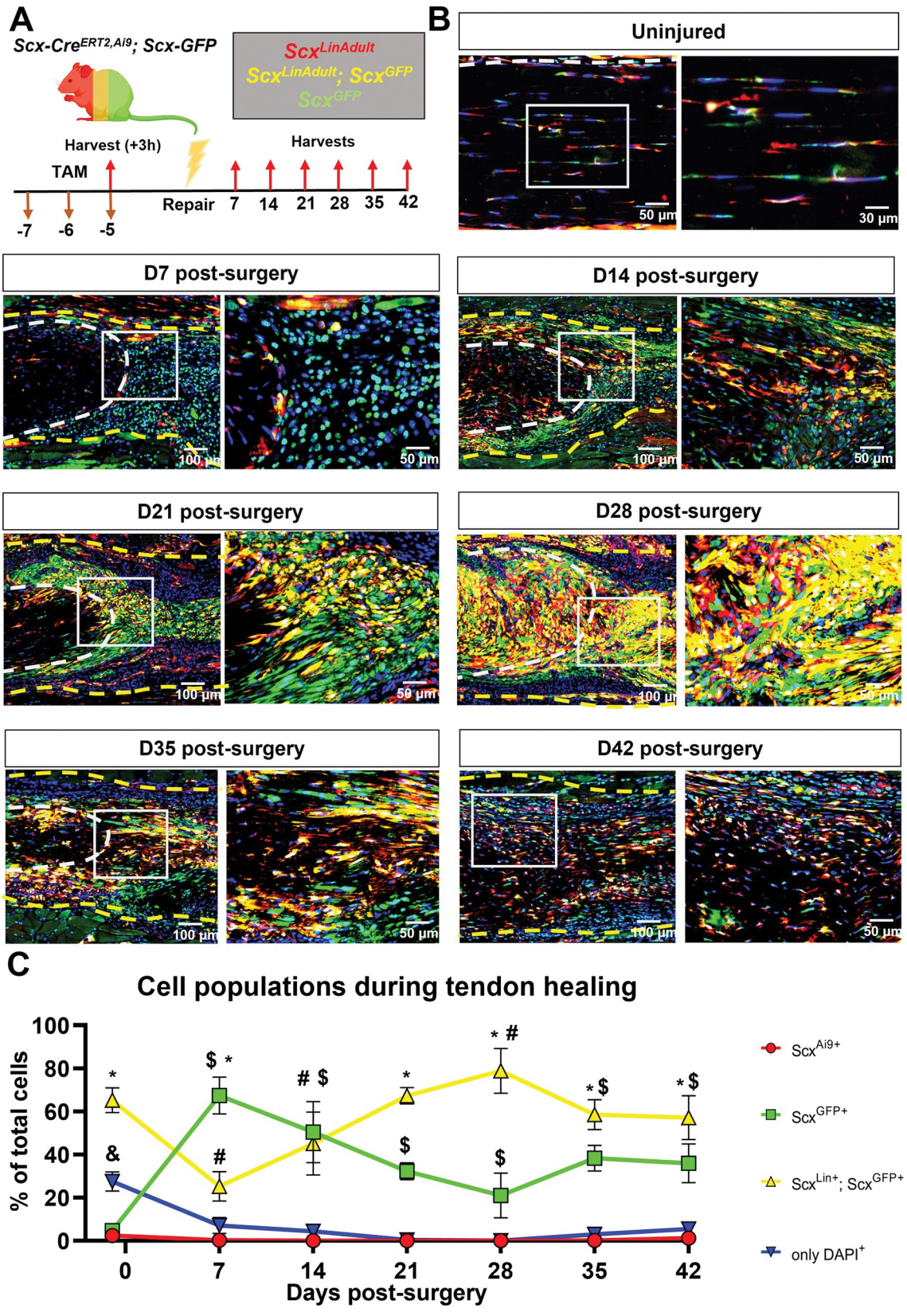
A
Scx-Cre^ERT2,Ai9; Scx-GFP
Scx^LinAdult
Scx^LinAdult; Scx^GFP
Scx^GFP
Harvest (+3h)
TAM
Harvests
Repair
7
14
21
28
35
42
-7
-6
-5
B
Uninjured
50 µm
30 µm
D7 post-surgery
D14 post-surgery
D21 post-surgery
D28 post-surgery
D35 post-surgery
D42 post-surgery
100 µm
50 µm
C
Cell populations during tendon healing
% of total cells
Days post-surgery
Scx^Ai9+
Scx^GFP+
Scx^Lin+; Scx^GFP+
only DAPI+

Fig 1. *Scx*^{Lin} cells continuously expand with additonal cells expressing *Scx* during tendon healing. A. Schematic of the mouse model used and timeline for tamoxifen injections, tendon surgeries, and tissue harvesting. **B.** Hind paws from *Scx-Cre*$^{ERT2, Ai9}$*; Scx-GFP* were probed Red Fluorescence Protein (RFP), Green Fluorescence Protein (GFP), and were counterstained with the nuclear dye DAPI. **C.** Cell density of *Scx*^{LinAdult}+, *Scx*^{GFP}+, *Scx*^{LinAdult}+;*Scx*^{GFP}+ and *only DAPI+*. White dashed lines represent the tendon stub. Yellow dashed lines represent the bridging tissue between the tendon stubs. per timepoint. N = 3–5 per timepoint. Significance was set to $p<0.05$. * represents a significant difference between *Scx*^{LinAdult}+;*Scx*^{GFP}+ and *Scx*^{GFP}+ at any given timepoint. **$** represents a significant differences in the *Scx*^{GFP}+ population during healing relative to uninjured controls. **#** represents a significant difference in *Scx*^{LinAdult}+;*Scx*^{GFP}+during healing relative to uninjured controls. **&** represents a significant difference of only *DAPI+* compared to the rest of the cell populations at a given timepoint.

https://doi.org/10.1371/journal.pone.0274227.g001

the healing timecourse (D7 through D42 post-surgery) compared to injured controls, and finally, how *Scx*^{GFP}+ change during the healing timecourse compared to injured controls. We have also provided a comprehensive statistical testing list with all possible comparisons between cell populations and timepoints to answer other scientific questions regarding the dynamics of the above cell populations during homeostasis and healing (**S1 Table**).

During homeostasis (10–12 weeks old), *Scx*^{LinAdult}+;*Scx*^{GFP}+ cells were the predominant population (65.3% of total cells), followed by *Scx*^{LinAdult}-;*Scx*^{GFP}- *cells* (27.51% of total cells), *Scx*^{LinAdult}-;*Scx*^{GFP}+ cells (4.72% of total cells), and finally *Scx*^{LinAdult}+;*Scx*^{GFP}- cells (2.47% of total cells) **(Fig 1B and 1C; S1 Table).** These data suggests that indeed the cell composition of homeostatic FDL tendons is heterogeneous with *Scx*^{LinAdult}+;*Scx*^{GFP}+ cells being the predominant population.

By D7 post-surgery, a substantial shift in the composition of the tenocyte cell enviornment was observed, with *Scx*^{LinAdult}-;*Scx*^{GFP}+ cells being the predominant population (67.4% of total cells), while *Scx*^{LinAdult}+;*Scx*^{GFP}+ cells accounted for 25.24% of the total cells **(Fig 1B and 1C; S1 Table).** Interestingly, there was a continuous decrease in the proportion of *Scx*^{LinAdult}-;*Scx*^{GFP}+ cells from D7 (67.4% of total cells) to D28 (21.03% of total cells) post-surgery. In parallel, the *Scx*^{LinAdult}+;*Scx*^{GFP}+ population continuously expanded from D7 (25.24% of total cells) to D28 (78.88% of total cells) post-surgery. Finally, the overall *Scx*^{Lin} pool (defined as the sum of *Scx*^{LinAdult}+;*Scx*^{GFP}+ and *Scx*^{LinAdult}+;*Scx*^{GFP}-) was substantially increased from homeostasis (72.48% of total cells) in response to injury at D28 post-surgery (99.92% of total cells) **(Fig 1B and 1C; S1 Table).**

From D35 through D42 post-surgery, the proportion of cells that were *Scx*^{LinAdult}+;*Scx*^{GFP}+ progressively decreased (D35:58.49%; D42: 57.18% of total cells) toward the levels observed during homeostasis (65.23% of total cells) **(Fig 1B and 1C; S1 Table).** In addition, at D35 and D42 there was an expansion of the *Scx*^{LinAdult}-;*Scx*^{GFP}- population **(Fig 1B and 1C; S1 Table).** Taken together, these data suggest that during the late stages of healing, the cell composition of the healing tendon begins to shift back toward the composition that is observed during homeostasis.

Scx expression is required for maintenance of myofibroblast (αSMA+) cells during tendon healing

We have previously shown that αSMA+ myofibroblasts are primarily derived from the broad *Scx*^{Lin} pool during adult tendon healing [9]. To get a better understanding of the dynamics of αSMA+ myofibroblast presence and their relationship to active *Scx* expression and the adult *Scx*^{LinAdult} pool during healing, we utilized the inducible *Scx-Cre*^{ERT2,Ai9}*; Scx*^{GFP} reporter mouse model and tracked the dynamics between *aSMA+* and *Scx*^{GFP}+(cells actively expressing Scx at the time of harvest) **(Fig 2A)** as well as *aSMA+* and adult *Scx*^{LinAdult}+ cells between D7 until D42 post-surgery **(S1 Fig).**

By D7 post-surgery, there were virtually no αSMA+ myofibroblasts in the healing tendons **(Fig 2A and 2B).** However, from D14 to D21, there was a substantial increase in αSMA+ cells

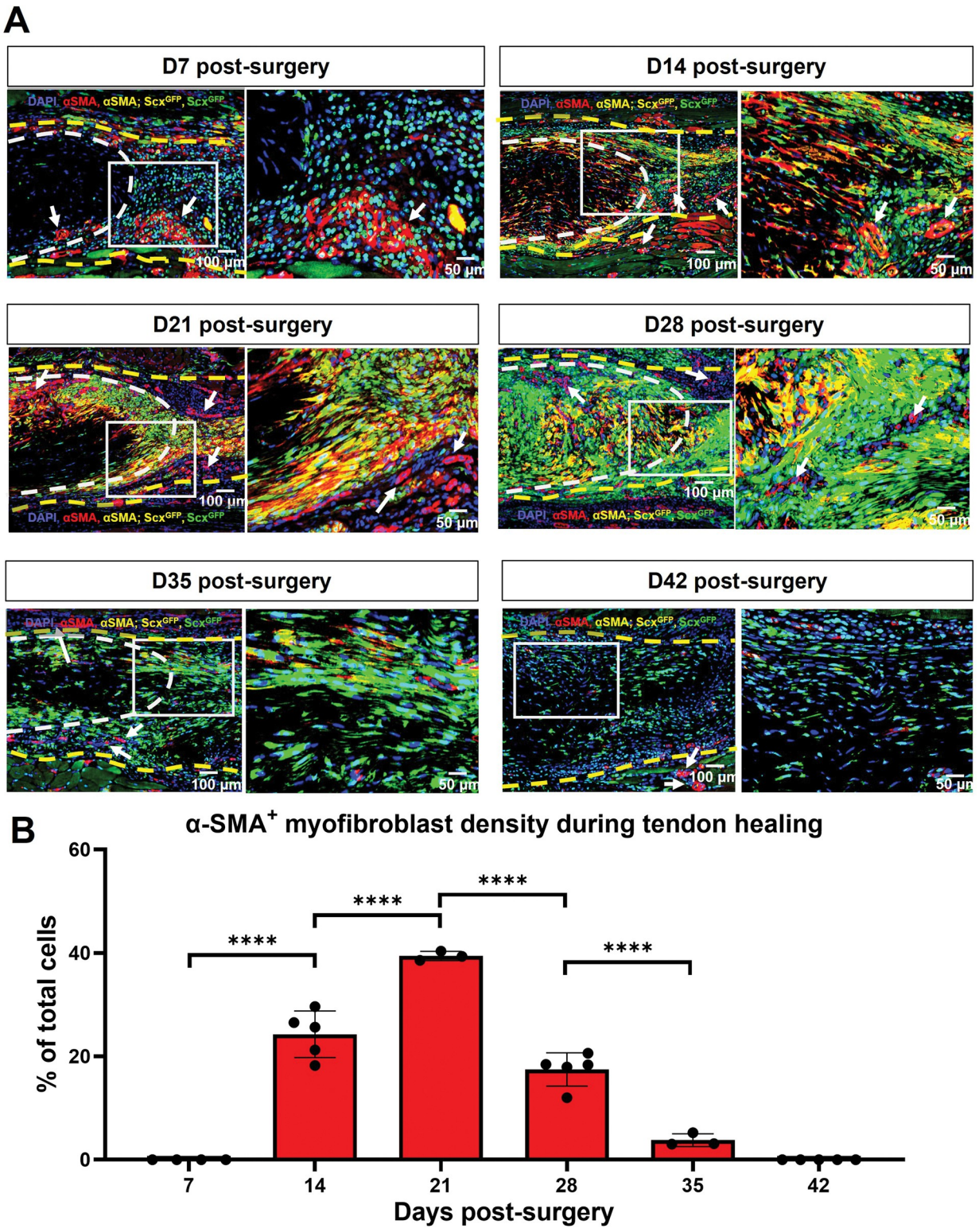

Fig 2. αSMA myofibroblasts are transiently present between D14 and D35 post-surgery and retain Scx expression. A. Hind paws from the *Scx-Cre*^{ERT2,Ai9}*; Scx*^{GFP}mice were probed with Green Fluorescence Protein (GFP) to visualize *Scx*^{GFP}+ cells, stained with αSMA to visualize myofibroblasts, and were counterstained with the nuclear dye DAPI. White dashed lines represent the tendon stub. Yellow dashed lines represent the bridging tissue between the tendon stubs. White arrows represent blood vessels. **B.** Cell density of *a*SMA+ cells overtime. Significance was set to $p<0.05$. **** represents $p<0.0001$. N = 3–5 per timepoint.

https://doi.org/10.1371/journal.pone.0274227.g002

in the healing tendon with nearly all αSMA+ cells actively expressing *Scx* (Fig 2A and 2B). At D28 and D35 post-surgery, *aSMA*+ cells persisted, and *Scx* expression was retained, however, the presence of *aSMA*+ was markedly reduced relative to D14 and D21 (Fig 2A and 2B). Finally, by D42, there were no *aSMA*+ cells in the injured tendons (Fig 2A and 2B). In terms of the adult $Scx^{LinAdult}$ contribution to myofibroblast fate, some *a*SMA+cells were derived from the adult $Scx^{LinAdult}$ population between D14 and D35 post-surgery (S1 Fig), though this population represents only a small fraction of myofibroblasts.

Healing DTR^{ScxLin} tendons exhibit deficits in structural mechanical and material properties

To define the requirement of the broad Scx^{Lin} cell pool during the proliferative phase of tendon healing, we utilized the *Scx-Cre+; Rosa-DTR*$^{F/+}$ (DTR^{ScxLin}) mice to deplete Scx^{Lin} cells between D14 and D18 post-surgery. For controls, we utilized the *Scx-Cre-; Rosa-DTR*$^{F/+}$ (WT). All mice received 5 consecutive local injections of Diphtheria Toxin (DT) in the injured tendon area and were harvested at D28 post-surgery (Fig 3A).

We have previously shown that intact DTR^{ScxLin} and WT FDL tendons exhibit no changes in biomechanical properties [7]. To assess whether Scx^{Lin} cells are required to restore tendon biomechanical properties during the proliferative healing phase, we quantified structural mechanical properties (peak load, stiffness) and material properties (peak stress, tangent modulus) (Fig 3B–3F). DTR^{ScxLin} tendons exhibited a 21.33% ($p<0.001$) increase in CSA compared to WT littermates (Fig 3B). The peak load of DTR^{ScxLin} tendons exhibited a trending decrease ($p = 0.06$) compared to WT (Fig 3C). The peak stress of DTR^{ScxLin} tendons was significantly decreased by 43.63% ($p<0.001$) compared to WT littermates (Fig 3D). As for stiffness, DTR^{ScxLin} tendons demonstrated a significant 48.72% decrease ($p<0.01$) compared to WT (Fig 3E). Finally, DTR^{ScxLin} tendons had a 61.94% ($p<0.0001$) decrease in tangent modulus compared to WT repairs (Fig 3F). Collectively, these data suggest that Scx^{Lin} cells are required for restoration of tendon biomechanics during healing.

Bulk RNA-seq reveals enrichment of pathways related to ECM synthesis and organization, cell-matrix adhesion, and cellular proliferation in DTR^{ScxLin} tendons

To better define the biological mechanisms associated with impaired healing in DTR^{ScxLin} tendon repairs, we performed bulk RNA-seq and assessed changes in the transcriptomic profile between DTR^{ScxLin} and WT tendons at D28. Scx^{Lin} cell depletion between D14-18 post-surgery resulted in a significant transcriptomic shift of healing tendons with 197 genes significantly increased and 269 genes significantly decreased in DTR^{ScxLin} compared to WT tendons (Fig 4A–4C). GO analysis via *Enrichr* identified multiple biological pathways that were significantly enriched in the DTR^{ScxLin} tendons based on the upregulated genes (Fig 4D). In specific, there were three main pathways enriched related to ECM (*TGF-β regulation of ECM* and *Collagen biosynthesis and modifying enzymes)*, cell-ECM adhesion (*Focal adhesion*, *ECM-receptor interaction)*, and cell mitosis/proliferation (*Cell cycle*: *G1/S Check point)* (Fig 4D).

Genes related to each enriched pathway were identified after screening all the significantly upregulated genes in DTR^{ScxLin} tendons using *StringDB*. For the ECM-related pathway, a total of 25 genes were identified and were expressed at significantly higher levels in all three different biological groups in DTR^{ScxLin} compared to WT tendons (Fig 4E). To assess any potential interactions between the ECM-related genes, *StringDB* was utilized and it was found that many of those genes do interact with each other (e.g. *Serpine1*, *Adamts16*, *Fbn1*, *Mfap5*, *Lox*, *Col5a1*, *Thbs1*, *Adamts1*, *Spon1*, *Adamts14*, *Col5a3*, *Postn*, *Aspn*, and *Ogn)* while other ECM-

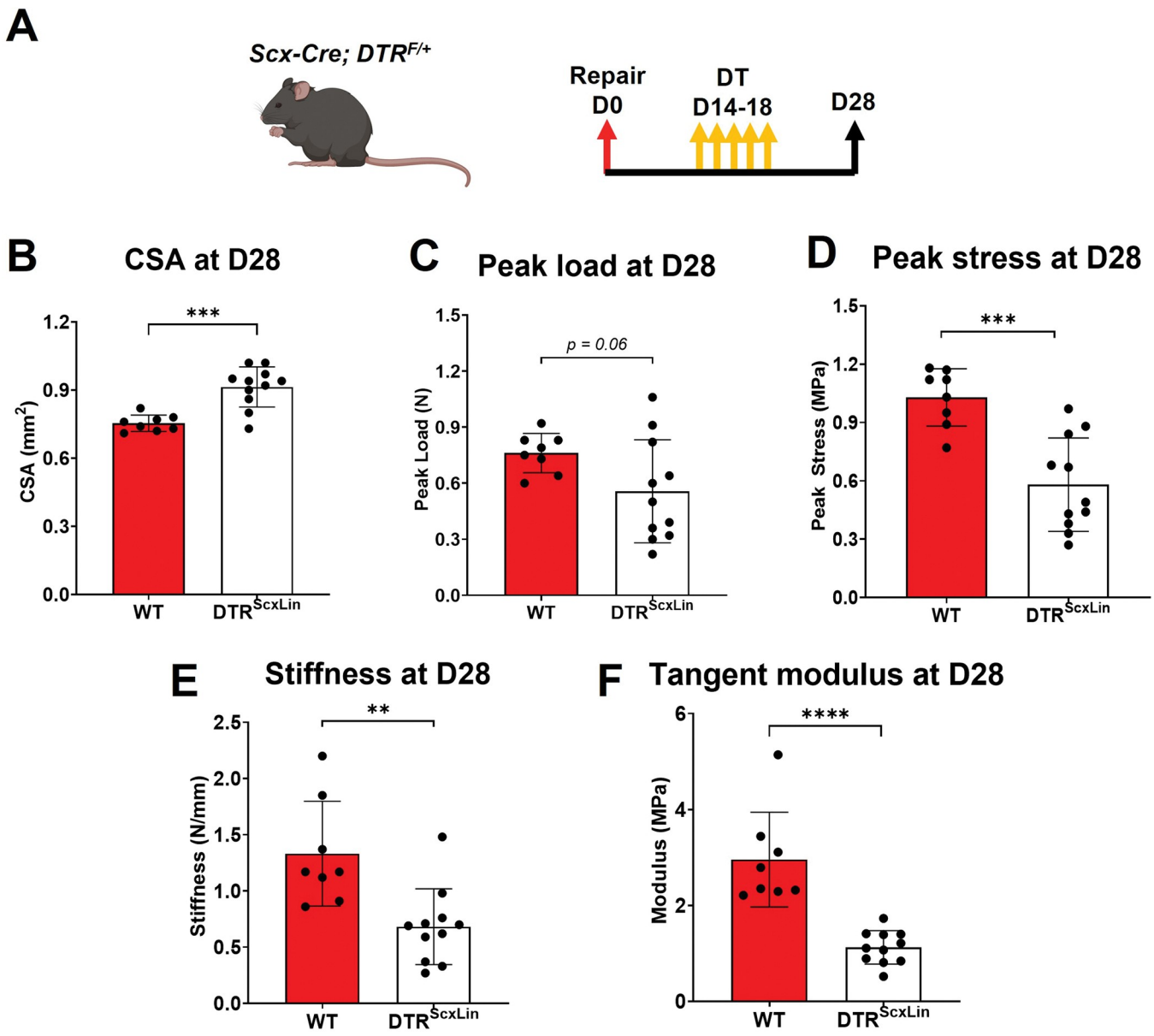

Fig 3. DTR^{ScxLin} tendons exhibit significant deficits in biomechanical properties. A. Schematic of the mouse model used and experimental timeline. CSA **(B)**, peak load **(C)**, peak stress **(D)**, stiffness **(E)**, and tangent modulus **(F)** of the the D28 DTR^{ScxLin} vs WT tendons. Student's t-test was utilized for statistical testing. N = 8–11 per genotype. **:p<0.01; ***:p<0.001; ****:p<0.0001.

https://doi.org/10.1371/journal.pone.0274227.g003

related genes did not exhibit interactions with the rest of the genes (e.g. *Thbs4*, *Epyc*, *Col8a1*, *Col24a1*, *Lama4*) (Fig 4F). Finally, GO analysis identified pathways related to *angiogenesis*, *regulation of TGFβ receptor pathway*, *biosynthesis of glycosaminoglycans (GAGs)*, and *ECM organization* were significantly enriched in DTR^{ScxLin} repairs (Fig 4G). Regarding the second main pathway enriched (*cell-ECM adhesion*, *Fig 4D*), a total of 14 genes were identified (Fig 4H). Analysis of the interaction of those proteins with each other showed that only *Spon1*, *Thbs1*, and *Vcam1* seem to have some interaction with each other (Fig 4I). GO analysis identified pathways related to *positive regulation of wound healing and epithelial cell migration*, *GAG*

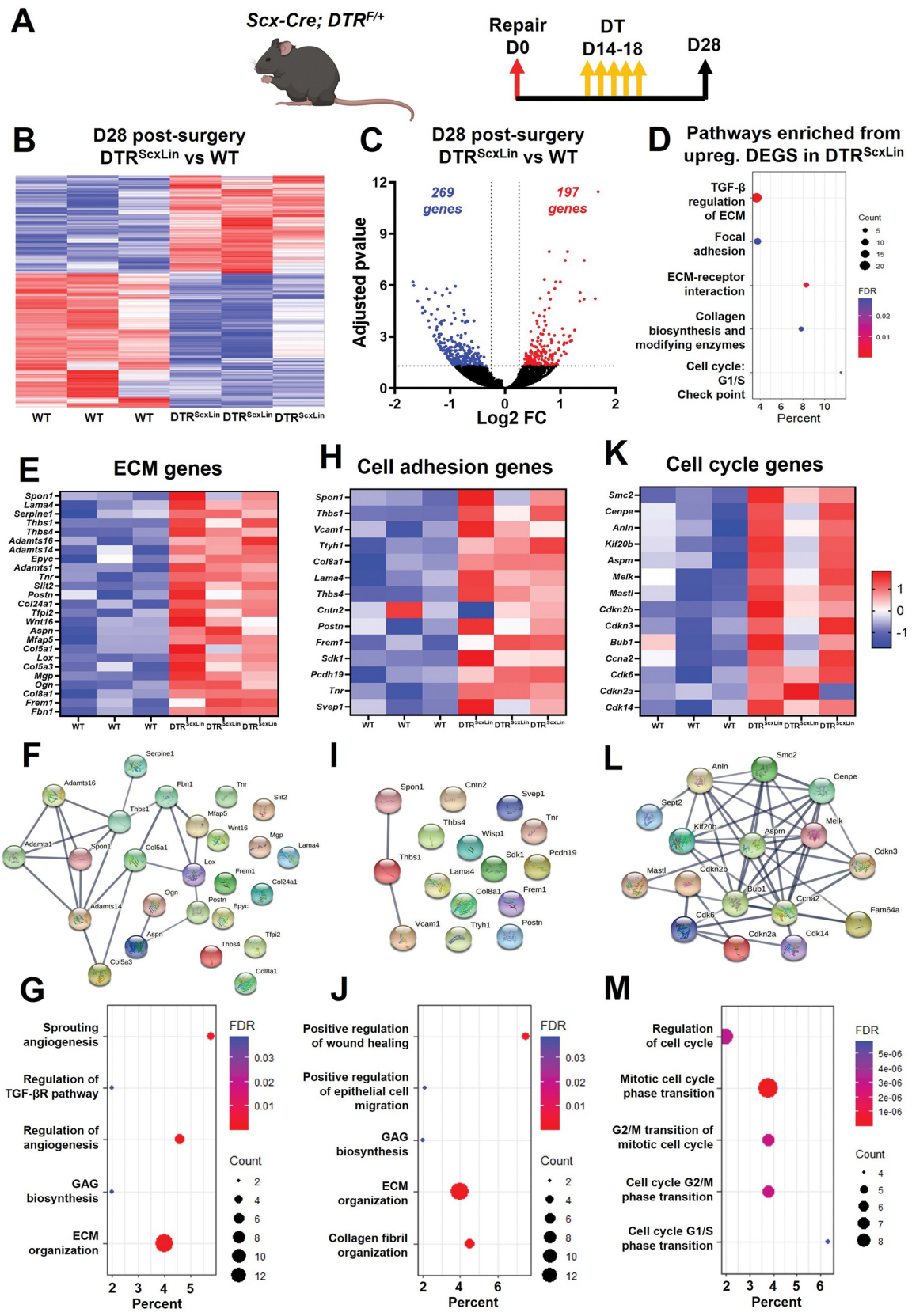
A
Scx-Cre; DTR^F/+
Repair
D0
DT
D14-18
D28
B
D28 post-surgery
DTR^ScxLin vs WT
WT
WT
WT
DTR^ScxLin
DTR^ScxLin
DTR^ScxLin
C
D28 post-surgery
DTR^ScxLin vs WT
269
genes
197
genes
Adjusted pvalue
Log2 FC
D
Pathways enriched from
upreg. DEGS in DTR^ScxLin
TGF-β
regulation
of ECM
Focal
adhesion
ECM-receptor
interaction
Collagen
biosynthesis and
modifying enzymes
Cell cycle:
G1/S
Check point
Count
FDR
Percent
E
ECM genes
Spon1
Lama4
Serpine1
Thbs1
Thbs4
Adamts16
Adamts14
Epyc
Adamts1
Tnr
Slit2
Postn
Col24a1
Tfpi2
Wnt16
Aspn
Mfap5
Col5a1
Lox
Col5a3
Mgp
Ogn
Col8a1
Frem1
Fbn1
H
Cell adhesion genes
Spon1
Thbs1
Vcam1
Ttyh1
Col8a1
Lama4
Thbs4
Cntn2
Postn
Frem1
Sdk1
Pcdh19
Tnr
Svep1
K
Cell cycle genes
Smc2
Cenpe
Anln
Kif20b
Aspm
Melk
Mastl
Cdkn2b
Cdkn3
Bub1
Ccna2
Cdk6
Cdkn2a
Cdk14
F
Serpine1
Adamts16
Fbn1
Tnr
Slit2
Thbs1
Mfap5
Wnt16
Mgp
Lama4
Adamts1
Spon1
Col5a1
Lox
Frem1
Col24a1
Ogn
Postn
Epyc
Adamts14
Aspn
Thbs4
Tfpi2
Col5a3
Col8a1
I
Spon1
Cntn2
Svep1
Tnr
Thbs4
Wisp1
Thbs1
Sdk1
Pcdh19
Lama4
Col8a1
Frem1
Vcam1
Ttyh1
Postn
L
Smc2
Anln
Cenpe
Sept2
Kif20b
Aspm
Melk
Cdkn3
Mastl
Cdkn2b
Bub1
Ccna2
Fam64a
Cdk6
Cdkn2a
Cdk14
G
Sprouting
angiogenesis
Regulation of
TGF-βR pathway
Regulation of
angiogenesis
GAG
biosynthesis
ECM
organization
FDR
Count
Percent
J
Positive regulation
of wound healing
Positive regulation
of epithelial cell
migration
GAG
biosynthesis
ECM
organization
Collagen fibril
organization
FDR
Count
Percent
M
Regulation
of cell cycle
Mitotic cell cycle
phase transition
G2/M transition of
mitotic cell cycle
Cell cycle G2/M
phase transition
Cell cycle G1/S
phase transition
FDR
Count
Percent

Fig 4. DTR^{ScxLin} tendons exhibit enriched biological pathways related to ECM synthesis and organization, cell-ECM receptor interaction, and cellular mitosis/proliferation. A. Schematic of the mouse model used and timeline for tendon surgeries, DT injections, and tissue harvesting. **B.** Heatmap of all significantly different genes between D28 DTR^{ScxLin} and WT tendons. **C.** Volcano plot of all the significantly different genes between D28 DTR^{ScxLin} and WT tendons. **D.** Enriched biological pathways from the upregulated genes in D28 DTR^{ScxLin} relative to WT tendons. **E.** Heatmap with all the ECM **(E)**, cell adhesion **(F)**, and cell cycle **(G)** genes significantly upregulated in D28 DTR^{ScxLin} tendons. **H.** Protein-protein communication of all the ECM **(H)**, cell adhesion **(I)**, and cell cycle **(J)** genes significantly upregulated in D28 DTR^{ScxLin} tendons. N = 3 per genotype.

https://doi.org/10.1371/journal.pone.0274227.g004

biosynthesis, *ECM organization*, and *collagen fibril organization* significantly enriched in DTR^{ScxLin} tendons (**Fig 4J**). Finally, for *cell mitosis/proliferation* (**Fig 4D**), screening using *StringDB* identified a total of 14 genes (**Fig 4K**). Interaction analysis demonstrated that all the cell mitosis related genes interact with each other, suggesting that they all follow the same mechanisms for cellular proliferation (**Fig 4L**). GO analysis identified pathways related to *regulation of cell cycle*, *mitotic cell cycle phase transition*, *G1/S and G2/M transition of mitotic cell cycle* were significantly enriched for DTR^{ScxLin} tendons (**Fig 4M**).

Taken together, these data suggest that D28 DTR^{ScxLin} tendons actively synthesizing ECM molecules related to wound closure. In parallel, there is cell proliferation (potentially of *Scx^{Lin}* cells [26]) in the healing DTR^{ScxLin} tendons that may be an attempt to increase cell density and to further aid in the wound closure. Such pathways are usually enriched when a tissue is within the proliferative healing phase [27–30]. Considering that *Scx^{Lin}* cell depletion was performed between D14-18 post-surgery, which is firmly in the proliferative phase, these data suggest that there is a stagnation of the healing response around the time of depletion (D14-18).

To validate that the healing response of D28 DTR^{ScxLin} tendons was stalled in a manner consistent with the molecular program of the proliferative phase, we conducted additional analysis of bulk RNA-seq data from our previously published study [7] from WT tendons at D14 post-surgery (proliferative phase) compared to WT at D28 post-surgery (remodeling phase) (**S2 Fig**). GO analysis of enriched pathways and biological processes based on all genes that were significantly increased in the D14 post-surgery (proliferative phase), showed that pathways and biological processes related to ECM synthesis and organization, cell-ECM adhesion, and cell proliferation/ mitosis were significantly activated (**S2A–S2J Fig**).

Bridging matrix of DTR^{ScxLin} tendons exhibits less mature collagen fibrils and high amount of proteoglycans and glycoproteins

To better understand the morphological features that occur concomitant with mechanical deficits and transcriptional shifts in DTR^{ScxLin} healing tendons, we performed Alcian Blue Hematoxylin Orange Green (ABHOG) staining and it revealed that indeed, the bridging tissue of D28 DTR^{ScxLin} tendons exhibited an impaired matrix quality compared to D28 WT tendons (**Fig 5B**). More specifically, DTR^{ScxLin} tendons exhibited thinner and more immature collagen fibrils, and increased staining of proteoglycans/glycoproteins (PGs/GPs) compared to WT tendons (**Fig 5B**), consistent with our bulk RNA-seq data (**Fig 4**). SHG imaging further validated the absence of mature collagen fibrils in DTR^{ScxLin} tendons relative to WT repairs (**Fig 5C**). Periostin (Postn) and Thrombospondin 4 (Thbs4) were among the significantly upregulated PGs/GPs in DTR^{ScxLin} tendons repairs relative to WT controls (**Fig 5E and 5H**). Immunofluorescence demonstrated significantly increased Postn (**Fig 5D and 5E**) and Thbs4 (**Fig 5F and 5G**) expression occurred in DTR^{ScxLin} tendons repairs relative to WT (**Fig 5D**). Taken together, these data suggest that *Scx^{Lin}* cells are required during the proliferative healing phase for matrix synthesis and maturation/remodeling, and their absence substantially impairs the composition, structure, and function of during tendon healing.

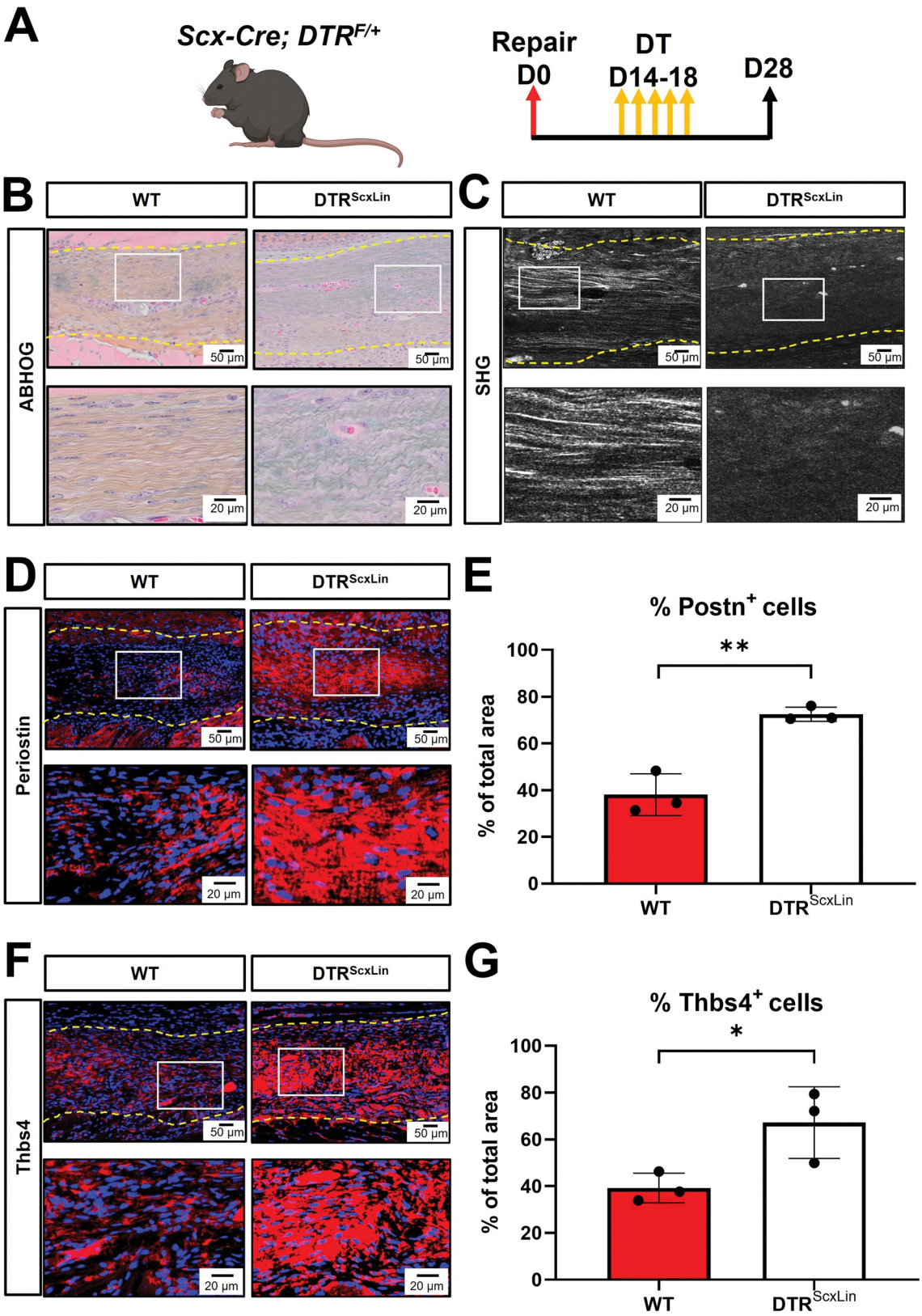

Fig 5. DTR^{ScxLin} tendons exhibit an immature bridging matrix tissue at D28 post-surgery. A. Schematic of the mouse model used and timeline for tendon surgeries, DT injections, and tissue harvesting. **B.** ABHOG staining to visualize the structure and organization

of the healing DTR^{ScxLin} vs WT tendons. **C.** SHG imaging to visualize mature collagen fibrils in the healing DTR^{ScxLin} vs WT tendons. **D.** Periostin staining (red) of D28 DTR^{ScxLin} vs WT tendons. **E.** Quantification of Periostin+ immunostaining area in the D28 DTR^{ScxLin} vs WT tendons. **F.** Thrombospondin 4 staining (red) of D28 DTR^{ScxLin} vs WT tendons. **G.** Quantification of Thrombospondin 4 + immunostaining area in the D28 DTR^{ScxLin} vs WT tendons. Nuclei are stained with DAPI (blue). N = 3 per genotype.

https://doi.org/10.1371/journal.pone.0274227.g005

DTR^{ScxLin} tendons fully restore their biomechanical properties by D56 post-surgery

To investigate whether the structure-function deficits during healing following *Scx^{Lin}* depletion (at D14-18) are transient or permanent, healing tendons were harvested for biomechanical testing at D56 post-surgery (late remodeling healing phase) (**Fig 6A**).

DTR^{ScxLin} tendons exhibited a 17.74% ($p<0.05$) increase in CSA compared to WT littermates (**Fig 6B**). The peak load, peak stress, stiffness, and tangent modulus of DTR^{ScxLin} tendons were not significantly different ($p>0.05$) compared to WT (**Fig 6C–6F**). These data suggest that in the long-term DTR^{ScxLin} tendons are able to restore structural mechanical and

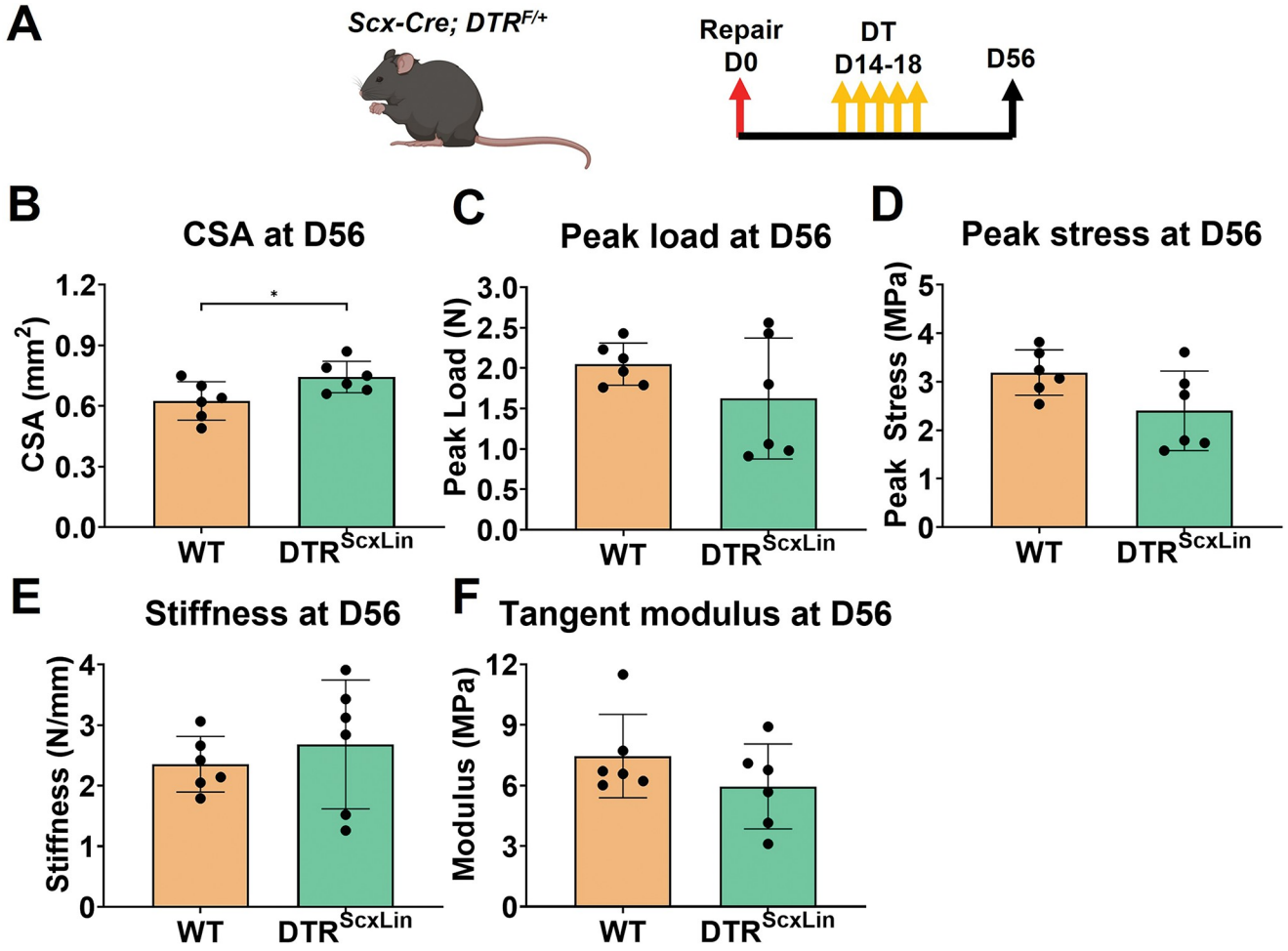

Fig 6. DTR^{ScxLin} tendons fully restore biomechanical propertes by D56 post-surgery. A. Schematic of the mouse model used and timeline for tendon surgeries, DT injections, and tissue harvesting. CSA **(B)**, peak load **(C)**, peak stress **(D)**, stiffness **(E)**, and tangent modulus **(F)** of the the D56 DTR^{ScxLin} vs WT tendons. Student's t-test was utilized for statistical testing. N = 6 per genotype. **:$p<0.01$; ***:$p<0.001$; ****:$p<0.0001$.

https://doi.org/10.1371/journal.pone.0274227.g006

material properties during healing, however the retained increase in CSA suggests a potential lack in further remodeling of the scar tissue.

Discussion

Here, we first characterized the dynamics of two major subpopulations of the broad Scx^{Lin} cell pool (adult $Scx^{LinAdult}$ and Scx^{GFP} cells) during tendon healing, and established that new *Scx*+ cells are continuously added to the overall Scx^{Lin} pool from the early proliferative (D7) to the remodeling phase (D28) of healing. Next, we also demonstrated the dynamics αSMA+ myofibroblasts and their relationship to Scx^{GFP} *(*cells actively expressing *Scx* at the time of harvest*)* cells throughout healing. Almost all αSMA myofibroblasts retained *Scx* expression for the duration of myofibroblast presence during healing, suggesting a potential requirement for Scx expression to maintain myofibroblast fate. No αSMA^{+} myofibroblasts were identified during homeostasis (prior to injury) [7]. Next, we investigated the function of a subset of the broad Scx^{Lin} pool by inducibly depleting Scx^{Lin} cells during the proliferative phase and found that Scx^{Lin} cells are required for ECM synthesis, organization, and restoration of tendon biomechanics. Strikingly, we found that Scx^{Lin} depletion from D14-18 caused a temporary stagnation of the healing response, stalling DTR^{ScxLin} tendons in the proliferative phase of healing even at D28 post-surgery. However, this stagnation was temporary such that by D56, mechanical properties were restored to the same level as WT repairs, suggesting that DTR^{ScxLin} tendons underwent successfully through the remodeling phase.

Disrupting tendon homeostasis via acute injury and repair resulted in significant shifts in the cell environment. By D7, $Scx^{LinAdult}$-; Scx^{GFP}+ cells that expressed *Scx* in response to injury, were the predominant population in the healing tendons. Although their source is not clear, it could be from the $Scx^{LinAdult}$-;Scx^{GFP}- population that is present during homeostasis. Indeed, recent findings from our lab and others have identified multiple tenocytes during homeostasis that do not express *Scx* but express markers related to wound healing and ECM synthesis [14,15,26,31]. Another alternative source could be epitenon-derived cells that migrate into the healing tendon. Indeed, we previously identified multiple *Scx*- epitenon cell subpopulations in healthy FDL tendons [14].

$Scx^{LinAdult}$-; Scx^{GFP}+ cells were identified as the predominant population between D7 and D14. Previously, we have shown that during these timepoints, the initital bridging tissue that connects the tendon stubs is formed by Scx^{Lin} cells [8,26]. From D14 to D28 post-surgery (proliferative and remodeling phase), the proportion of $Scx^{LinAdult}$-; Scx^{GFP}+ cells was reduced, while the $Scx^{LinAdult}$+; Scx^{GFP}+ population continuously expanded. Taken together, these data suggest that $Scx^{LinAdult}$-; Scx^{GFP}+ and $Scx^{LinAdult}$+; Scx^{GFP}+ cells may have distinct functions during tendon healing. More specifically, $Scx^{LinAdult}$-; Scx^{GFP}+ cells may be responsible for synthesizing the initial bridging scar tissue. In contrast, $Scx^{LinAdult}$+; Scx^{GFP}+ cells may be responsible for remodeling and organization of the bridging scar tissue.

Myofibroblasts demonstrated a transient presence, peaking in the proliferative phase (D21), decreasing during the remodeling phase (D28 through D35), and fully resolving by the later remodeling phase (D42).

During their presence in healing tendons, almost all myofibroblasts were *Scx*+ and retained their *Scx* expression until they were resolved, suggesting that *Scx* expression is required for αSMA myofibroblast maintenance during tendon healing. In support to this finding, previous studies in cardiac fibroblasts have shown that *Scx* expression is both required and necessary for the synthesis of αSMA protein and conversion of fibroblasts to myofibroblasts [32–35]. In specific, Bagchi *et al*., utilized an *in vitro* system for *Scx* gain- or loss- of function in primary cardiac fibroblasts and their effect on αSMA expression [35]. They found that *Scx* knockdown

reduced αSMA expression and incorporation into stress fibers while overexpression of *Scx* resulted in further induction of αSMA expression and production of stress fibers [35]. Moreover, we found that almost none of the *a*SMA$^+$ cells were derived from the $Scx^{LinAdult}$ cells at any timepoint post-surgery, similar to our previous findings [8].

To understand the requirements for the broad Scx^{Lin} cell population during the proliferative healing phase, we depleted these cells between D14 and D18 post-surgery and found that these cells are important for restoration of structure, composition, and function in healing tendons. In specific, the bridging matrix tissue of D28 DTR^{ScxLin} tendons was characterized by immature collagen fibrils, increased expression of multiple ECM glycoproteins and proteoglycans, and reduced structural mechanical and material properties. These data suggest that Scx^{Lin} cells play a key role in both the synthesis and remodeling of the ECM in the bridging tissue. In accordance to our findings, multiple studies have previously assumed that Scx^{Lin} cells are required during tendon healing for ECM synthesis, organization, and wound clousure [8,9,17,18,36]. However, in this study, we directly tested and identified the requirements of Scx^{Lin} cells during tendon healing.

GO analysis from bulk RNA-seq at D28 post-surgery demonstrated that pathways and biological processes related to ECM synthesis and organization, cell-ECM adhesion, and cell proliferation/mitosis were significantly enriched in DTR^{ScxLin} tendons. Interestingly, such pathways and biological processess are typically upregulated when tissues are going through the proliferative healing phase [27–30]. Indeed, GO analysis of bulk RNA-seq data between WT D14 (proliferative phase) and WT D28 (remodeling phase) post-surgery timepoints, revealed that pathways and biological mechanisms related to ECM synthesis and organization, cell-ECM adhesion, and cell proliferation/mitosis were significantly enriched in the D14 post-surgery tendons. In addition to the transcriptomic data, both the morphology and biomechanics of the D28 DTR^{ScxLin} tendons were almost identical with those of D14 WT tendons that we have previously published in separate studies [7,14,22,37,38]. Taking into account that Scx^{Lin} depletion was performed between D14-18 post-surgery, which is firmly in the proliferative phase, it suggests that with depletion, DTR^{ScxLin} tendons had become stagnant during healing, essentially stalling the healing process in the proliferative phase at least through D28 post-surgery. Next, we examined the long-term ability of DTR^{ScxLin} tendons to restore the healing process to that of WT. Indeed, at D56 post-surgery, DTR^{ScxLin} tendons were able to fully restore both their structural mechanical and material properties in the same levels as D56 WT tendons. This suggests that DTR^{ScxLin} tendons eventually progressed through the normal stages of healing including tissue remodeling, and suggests great plasticity of the healing process even when disrupted during the proliferative phase.

This study is not without limitations. First, although we distinguished between adult Scx^{Lin} and Scx^{GFP} cells during the different healing phases (D7 through D42 post-surgery), this depletion model targets both of these subpopulations. As such, it not possible to further decipher the requirements of specific subpopulations of cells in the overall Scx^{Lin} pool (e.g., roles of only the adult Scx^{Lin} cells) with this model. Previous efforts to deplete cells actively expressing *Scx* by using the inducible *Scx-*Cre^{ERT2} crossed to Rosa-DTA [39] mice resulted in insufficient recombination. Thus, in order to deplete specific subpopulations of Scx^{Lin} cells in a temporally-dependent manner, future work could utilize *Scx-*Cre^{ERT2};Rosa-DTR mice, although this model requires both TMX and DT administration, and discrepencies in labelling vs. depletion may be observed. Another limitation is the inability to quantify depletion efficiency at different timepoints post-surgery, as we have not included a *Scx*-reporter. Finally, by D56 post-surgery, although we showed restoration of the biomechanics of DTR^{ScxLin} tendons relative to WT, we do not have histological analysis of that timepoint. In the future, we are planning to assess histologically D56 DTR^{ScxLin} and WT groups.

Taken together, in this study, we first demonstrated in detail the dynamics of two major subpopulations of the broad Scx^{Lin} pool (adult Scx^{Lin} and Scx^{GFP} cells) during the entire tendon healing course. We next found that *Scx* expression is required for myofibroblast maintenance and in parallel provided clear evidence of the spatial and temporal presence of active myofibroblasts during tendon wound healing. Next, we directly tested the role of Scx^{Lin} cells by depleting them in the proliferative healing phase and found that they are required to produce and remodel ECM, as well as to restore tendon biomechanics. Their absence resulted in a temporary stagnation of healing response, though, long-term, DTR^{ScxLin} tendons eventually healed to the same extent as WT repairs.

Supporting information

S1 Fig. Temporal dynamics of $Scx^{LinAdult}$ cells and αSMA myofibroblasts during tendon healing A. Schematic of the mouse model used and timeline for tamoxifen injections, tendon surgeries, and tissue harvesting. **B.** Hind paws from *Scx-*$Cre^{ERT2,Ai9}$ mice were probed for Red Fluorescence Protein (RFP) to visualize $Scx^{LinAdult}$ cells, and αSMA-FITC to visualize myofibroblasts. All samples were counterstained with the nuclear dye DAPI. N = 3–5 per timepoint.
(TIF)

S2 Fig. FDL tendons in the proliferative phase exhibit enriched biological pathways related to ECM synthesis and organization, cell-ECM receptor interaction, and cellular mitosis/proliferation compared to FDL tendons in the remodeling phase. A. Schematic of the mouse model used and timeline for tendon surgeries, DT injections, and tissue harvesting. **B.** Volcano plot of all the significantly different genes between D28 vs D14 WT tendons. Enriched pathways **(C)** and biological processess **(D)** between D28 vs D14 WT tendons. **E.** Protein-protein communication of all the ECM **(E)**, cell adhesion **(G)**, and cell cycle **(I)** genes between D28 vs D14 WT tendons. Enriched pathways related ECM **(F)**, cell adhesion **(H)**, and cell cycle **(J)** between D28 vs D14 WT tendons.
(TIF)

S1 Table.
(TIFF)

S2 Table.
(TIFF)

Author Contributions

Conceptualization: Antonion Korcari, Alayna E. Loiselle.

Data curation: Antonion Korcari, Samantha Muscat.

Formal analysis: Antonion Korcari, Elizabeth McGinn, Mark R. Buckley, Alayna E. Loiselle.

Funding acquisition: Alayna E. Loiselle.

Investigation: Antonion Korcari, Alayna E. Loiselle.

Methodology: Antonion Korcari, Elizabeth McGinn, Mark R. Buckley, Alayna E. Loiselle.

Project administration: Antonion Korcari, Alayna E. Loiselle.

Resources: Mark R. Buckley, Alayna E. Loiselle.

Software: Antonion Korcari, Alayna E. Loiselle.

Supervision: Alayna E. Loiselle.

Validation: Mark R. Buckley, Alayna E. Loiselle.

Visualization: Antonion Korcari.

Writing – original draft: Antonion Korcari, Alayna E. Loiselle.

Writing – review & editing: Antonion Korcari, Mark R. Buckley, Alayna E. Loiselle.

References

1. Franchi M, Trirè A, Quaranta M, Orsini E, Ottani V: Collagen structure of tendon relates to function. *ScientificWorldJournal* 2007, 7:404–420.
2. Strickland JW: Flexor Tendon Injuries: I. Foundations of Treatment. *J Am Acad Orthop Surg* 1995, 3 (1):44–54. https://doi.org/10.5435/00124635-199501000-00006 PMID: 10790652
3. Aydin A, Topalan M, Mezdeği A, Sezer I, Ozkan T, Erer M, Ozkan S: [Single-stage flexor tendoplasty in the treatment of flexor tendon injuries]. *Acta Orthop Traumatol Turc* 2004, 38(1):54–59.
4. Caulfield RH, Maleki-Tabrizi A, Patel H, Coldham F, Mee S, Nanchahal J: Comparison of zones 1 to 4 flexor tendon repairs using absorbable and unabsorbable four-strand core sutures. *J Hand Surg Eur Vol* 2008, 33(4):412–417. https://doi.org/10.1177/1753193408090758 PMID: 18687826
5. Ackerman JE, Loiselle AE: Murine Flexor Tendon Injury and Repair Surgery. *J Vis Exp* 2016(115). https://doi.org/10.3791/54433 PMID: 27684281
6. Ackerman JE, Nichols AE, Studentsova V, Best KT, Knapp E, Loiselle AE: Cell non-autonomous functions of S100a4 drive fibrotic tendon healing. *Elife* 2019, 8. https://doi.org/10.7554/eLife.45342 PMID: 31124787
7. Best KT, Korcari A, Mora KE, Nichols AE, Muscat SN, Knapp E, et al: Scleraxis-lineage cell depletion improves tendon healing and disrupts adult tendon homeostasis. *Elife* 2021, 10:e62203.
8. Best KT, Loiselle AE: Scleraxis lineage cells contribute to organized bridging tissue during tendon healing and identify a subpopulation of resident tendon cells. *Faseb j* 2019, 33(7):8578–8587.
9. Best KT, Nichols AEC, Knapp E, Hammert WC, Ketonis C, et al: NF-κB activation persists into the remodeling phase of tendon healing and promotes myofibroblast survival. *Sci Signal* 2020, 13(658). https://doi.org/10.1126/scisignal.abb7209 PMID: 33203721
10. de la Durantaye M, Piette AB, van Rooijen N, Frenette J: Macrophage depletion reduces cell proliferation and extracellular matrix accumulation but increases the ultimate tensile strength of injured Achilles tendons. *J Orthop Res* 2014, 32(2):279–285.
11. Korcari A, Nichols AE, O'Neil M, Loiselle AE: Ligament and tendon tissue engineering. *Musculoskeletal Tissue Engineering* 2021: 81.
12. Korcari A, Przybelski SJ, Gingery A, Loiselle AE: Impact of aging on tendon homeostasis, tendinopathy development, and impaired healing. *Connective Tissue Research* 2022:1–13.
13. Nichols AEC, Best KT, Loiselle AE: The cellular basis of fibrotic tendon healing: challenges and opportunities. *Transl Res* 2019, 209:156–168. https://doi.org/10.1016/j.trsl.2019.02.002 PMID: 30776336
14. Korcari A, Nichols AEC, Loiselle AE: Depletion of Scleraxis-lineage cells accelerates tendon ECM aging and retains remodeling tenocytes that enhance tendon healing. *BioArxiv* 2022.
15. Kendal AR, Layton T, Al-Mossawi H, Appleton L, Dakin S, Brown R, et al: Multi-omic single cell analysis resolves novel stromal cell populations in healthy and diseased human tendon. *Sci Rep* 2020, 10 (1):13939.
16. Schweitzer R, Chyung JH, Murtaugh LC, Brent AE, Rosen V, Olson EN, et al: Analysis of the tendon cell fate using Scleraxis, a specific marker for tendons and ligaments. *Development* 2001, 128 (19):3855–3866.
17. Dyment NA, Hagiwara Y, Matthews BG, Li Y, Kalajzic I, Rowe DW: Lineage tracing of resident tendon progenitor cells during growth and natural healing. *PLoS One* 2014, 9(4):e96113. https://doi.org/10.1371/journal.pone.0096113 PMID: 24759953
18. Howell K, Chien C, Bell R, Laudier D, Tufa SF, Keene DR, et al: Novel Model of Tendon Regeneration Reveals Distinct Cell Mechanisms Underlying Regenerative and Fibrotic Tendon Healing. *Sci Rep* 2017, 7:45238. https://doi.org/10.1038/srep45238 PMID: 28332620
19. Murchison ND, Price BA, Conner DA, Keene DR, Olson EN, Tabin CJ, et al: Regulation of tendon differentiation by scleraxis distinguishes force-transmitting tendons from muscle-anchoring tendons. *Development* 2007, 134(14):2697–2708.

20. Pryce BA, Brent AE, Murchison ND, Tabin CJ, Schweitzer R: Generation of transgenic tendon reporters, ScxGFP and ScxAP, using regulatory elements of the scleraxis gene. *Dev Dyn* 2007, 236 (6):1677–1682.

21. Buch T, Heppner FL, Tertilt C, Heinen TJ, Kremer M, Wunderlich FT, et al: A Cre-inducible diphtheria toxin receptor mediates cell lineage ablation after toxin administration. *Nat Methods* 2005, 2(6):419–426.

22. Korcari A, Loiselle AE, Buckley MR: Characterization of scar tissue biomechanics during adult murine flexor tendon healing. *bioRxiv* 2021:2021. 2011.2009.467960. https://doi.org/10.1016/j.jmbbm.2022.105192 PMID: 35339739

23. Bah I, Kwak ST, Chimenti RL, Richards MS, J PK, Samuel Flemister A, et al: Mechanical changes in the Achilles tendon due to insertional Achilles tendinopathy. *J Mech Behav Biomed Mater* 2016, 53:320–328. https://doi.org/10.1016/j.jmbbm.2015.08.022 PMID: 26386166

24. Navarro J, Korcari A, Nguyen P, Bah I, AlKhalifa A, Fink S, et al: Method development and characterization of chick embryo tendon mechanical properties. *Journal of Biomechanics* 2022, 133:110970.

25. Korcari A, Buckley MR, Loiselle AE: Characterization of Scar Tissue Biomechanics During Adult Murine Flexor Tendon Healing. *SSRN Electronic Journal* 2021.

26. Ackerman JE, Best KT Muscat S, u C-L, Loiselle AE: 2021.

27. Voleti PB, Buckley MR, Soslowsky LJ: Tendon healing: repair and regeneration. *Annu Rev Biomed Eng* 2012, 14:47–71. https://doi.org/10.1146/annurev-bioeng-071811-150122 PMID: 22809137

28. Landén NX, Li D, Ståhle M: Transition from inflammation to proliferation: a critical step during wound healing. *Cell Mol Life Sci* 2016, 73(20):3861–3885.

29. Thomopoulos S, Parks WC, Rifkin DB, Derwin KA: Mechanisms of tendon injury and repair. *J Orthop Res* 2015, 33(6):832–839.

30. Yang G, Rothrauff BB, Tuan RS: Tendon and ligament regeneration and repair: clinical relevance and developmental paradigm. *Birth Defects Res C Embryo Today* 2013, 99(3):203–222. https://doi.org/10.1002/bdrc.21041 PMID: 24078497

31. Akbar M, MacDonald L, Crowe LAN, Carlberg K, Kurowska-Stolarska M, Stahl PL, et al: Single cell and spatial transcriptomics in human tendon disease indicate dysregulated immune homeostasis. *Ann Rheum Dis* 2021, 80(11):1494–1497.

32. Espira L, Lamoureux L, Jones SC, Gerard RD, Dixon IM, Czubryt MP: The basic helix-loop-helix transcription factor scleraxis regulates fibroblast collagen synthesis. *J Mol Cell Cardiol* 2009, 47(2):188–195.

33. Al-Hattab DS, Safi HA, Nagalingam RS, Bagchi RA, Stecy MT, Czubryt MP: Scleraxis regulates Twist1 and Snai1 expression in the epithelial-to-mesenchymal transition. *Am J Physiol Heart Circ Physiol* 2018, 315(3):H658–h668.

34. Eadie AL, Titus AJ, Brunt KR: Getting to the heart of myofibroblast differentiation: implications for scleraxis in ECM remodeling and therapeutic targeting. *Am J Physiol Heart Circ Physiol* 2018, 315(5): H1232–h1235.

35. Bagchi RA, Roche P, Aroutiounova N, Espira L, Abrenica B, Schweitzer R, et al: The transcription factor scleraxis is a critical regulator of cardiac fibroblast phenotype. *BMC Biol* 2016, 14:21. https://doi.org/10.1186/s12915-016-0243-8 PMID: 26988708

36. Dyment NA, Liu CF, Kazemi N, Aschbacher-Smith LE, Kenter K, Breidenbach AP, et al: The paratenon contributes to scleraxis-expressing cells during patellar tendon healing. *PLoS One* 2013, 8(3):e59944. https://doi.org/10.1371/journal.pone.0059944 PMID: 23555841

37. Neidlin M, Korcari A, Macheras G, Alexopoulos LG: Cue-signal-response analysis in 3d chondrocyte scaffolds with anabolic stimuli. *Annals of biomedical engineering* 2018, 46(2):345–353.

38. Korcari A, Buckley MR, Loiselle AE: Characterization of scar tissue biomechanics during adult murine flexor tendon healing. *J Mech Behav Biomed Mater* 2022, 130:105192. https://doi.org/10.1016/j.jmbbm.2022.105192 PMID: 35339739

39. Voehringer D, Liang HE, Locksley RM: Homeostasis and effector function of lymphopenia-induced "memory-like" T cells in constitutively T cell-depleted mice. *J Immunol* 2008, 180(7):4742–4753. https://doi.org/10.4049/jimmunol.180.7.4742 PMID: 18354198